Chalcogenide Letters Vol. 14, No. 11, November 2017, p. 499 - 510

TRIBOLOGICAL PROPERTIES OF NOVEL Cu/$NbSe_2$ COMPOSITES REINFORCED WITH REDUCED GRAPHENE OXIDE FILLER

J. F. LI[a], B. CHEN[a], Q. SHI[bc], C. LI[a], Y. CHU[d], C. LI[ab*]
[a]*School of Materials Science and Engineering, Jiangsu University, Key Laboratory of Tribology of Jiangsu Province, Zhenjiang, 212013, P. R. China*
[b]*School of Mechanical Engineering, Jiangsu University, 301, Xuefu Road, Zhenjiang, 212013, Jiangsu Province, P. R. China*
[c]*School of Mechanical Engineering, Zhenjiang Vocational Technical College, Zhenjiang, 212016, P. R. China*
[d]*School of Science, Jiangsu University of Science and Technology, Zhenjiang 212003,China*

Novel Cu-based composites with niobium selenide ($NbSe_2$) and reduced graphene oxide (RGO) were sucessfully fabricated using powder metallurgy method (PM). The physical and tribological behaviors of composites were systematically studied. It was found that compared with copper, Cu-based composites showed increased hardness and decreased density. Besides, Cu-based composites with 18wt.% $NbSe_2$ and 2wt.% RGO possessed the excellent tribological properties among all composites. According to experimental data analysis, a complete and dense tribo-film was formed on the worn surface, mainly composing of Fe_2O_3, CuO, Nb_2O_5, RGO and $NbSe_2$ thiner sheets exfoliated.

(Received September 19, 2017; Accepted November 27, 2017)

Keyword: Cu-based composites; $NbSe_2$; Reduced graphene oxide; Tribo-film

1. Introduction

Metallic matrix composites with excellent mechanical and tribological properties used as advanced enginering materials are the most promising materials in many industries. Especially, Cu-based composites have always attracted wide attention because of good thermal and electrical conductivities, good corrosion resistance, ease of process and low cost compared with all metallic materials[1-5]. Especially in tribology, the appliacation of copper matrix composites was limited greatly due to low hardness and poor anti-wear properties. Some researchers have reported that high loads or sliding speed led to severe damage to copper and its composites in the process of friction [6-8]. Therefore, it is the primary work to improve the tribological properties of copper and its composites by addition of transition metal dichalcogenides (MX_2)or graphite etc. However they also had many drawbacks which led to them not be used in the extremely environment. For example, graphite possesses the excellent lubricity, but its' poor performance in tribological properties would be experienced when in vacuum or dry environments. MoS_2 with exceptional low friction coefficient and wear rate was applied in vacuum circumstance. Furthermore, the hardness of graphite and MoS_2 is low, which seriously deteriorates the load-carrying capacity of composites. Therefore, it is vital to develop outstanding tribological properties for Cu-based composites to satisfy the requirements.

Transition metal dichalcogenides $NbSe_2$ has a hexagonal layered structure like MoS_2 and graphite, which has excellent self-lubricant property[9]. In the past few years, we have studied the tribological properties of $NbSe_2$ into metal matrix. Tang et al [10] have found that Cu/$NbSe_2$ composites containing appropriate $NbSe_2$ show low electrical resistivity and outstanding tribological behaviors. Chen et al [11], who have reported that the addition of copper coated CTNs

* Corresponding author: ljftxzq@163.com

and $NbSe_2$ in copper matrix would improve electrical property and tribological behavior of Cu-based composites. Zhang et al [12] have investigated that the plastic deformation of the substrate can be effectively decreased by filling $NbSe_2$ so that enhance the antifrction and antiwear behaviors of composites.

Recently, extensive attention is paid to graphene for its properties such as high electrical and thermal conductivity, high modulus, fracture strength[13]. With its excellent properties, the tribological properties of graphene have aslo been explored. The tribological properties of metal matrix composites containing graphene were reported in many previous papers. Xu et al [14] have found that TiAl matrix composites with multilayer graphene can drastically not only enhance the strength, but reduce friction coefficient and wear rate of composites. Zhang et al[15]have investigated that Fe-Ni matrix composites with MoS_2/RGO exhibits excellent antifriction properties due to the combined effects of solid lubricants and strengthening phase compared with Fe-Ni matrix. Unfortunately, no relevant reports about the investigation of $NbSe_2$ and graphene used in the Cu-based composites were found.

In this work, two lamellar materials, reduced graphene oxide (RGO) and $NbSe_2$ were prepared, and then were added into Cu matrix. And the corresponding reinforcing and lubricating mechanisms were discussed as well.

2. Experimental details

$NbSe_2$ were successfully prepared using solid state sintered technology and the fabrication process were described [16,17]. Exfoliation of graphite using the modified Hummer's method could synthesize successfully graphene oxide (GO)[18]. 4g graphite powder and 4g $NaNO_3$ were slowly added into 200 ml cooled (0^oC) concentrated H_2SO_4. The solution was stirred mechanically in a 1000 ml breaker. 30 g of $KMnO_4$ was slowly added into mixture with stirring, and the reaction lasted for about 90 min. After cooling down to room temperature, the mixture was slowly transferred into cold (0^oC) deionized water, followed by adding 30% H_2O_2 slowly until the solution changed into bright yellow. The solid product was centrifuged and washed for several times with 5% HCl solution and distilled water until the pH of the mixture was about 7. The GO nanosheets was obtained by drying in a vacuum oven at 60^oC for 8 h.

Five kinds of composites were prepared by powder metallurgy technique. And Table 1 listed the compositions (denoted as C, CN, CGN1, CGN2 and CGN3). Fig.1 shows the schematic illustration of fabrication process of specimen CGN1, CGN2 and CGN3. The prepared GO nanosheets was added into acetone and sonicated by ultrasonic dispersing technology for over 6h so that formed the homogeneous discretely suspension. As-prepared $NbSe_2$ were added into the aforemention suspension, which be mechanically stirred for 3 h. High-purity copper (50μm) powders was added and formed a powder slurry with stirring after the hydrazine hydrate was added slowly. The slurry was dried to form the freeze-dried composite powder by freezing and then kept under vacuum (1Pa) to remove the water.

Finally, the mixed powder was cold-presssed at 500 Mpa and sintered in a nitrogen atmosphere at 800^oC for 2h. As the temperature decreased to room temperature, the surface of specimens were processed for the following tests and analyses. For comparison, specimen C and CN were fabricated using the above fabrication process.

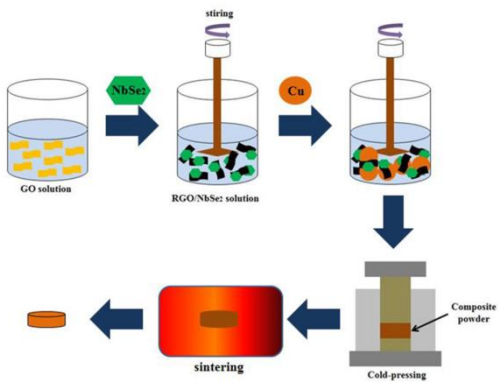

Fig.1. Schematic illustration of fabrication process of specimen CGN1, CGN2 and CGN3

2.1.Characterization

The phase composition of as-prepared specimens were identified by X-ray diffractometer (Bruker-AXS). The morphology of as-prepared powders were analyzed by SEM (JSM-7001F) equipped with EDS, TEM (JEOL-2010). The morphology and phase compositions of worn surface of specimens was examined via SEM (S-3400N) equipped with EDS and Laser Raman Spectrometer (DXR). The elemental states of wear scars were analyzed by XPS (Thermo ESCALAB 250XL).

Archimedes's principle was employed to measure the composite densities according to ASTMC-20 standard. The hardness of specimens was estimated by an MH-5 Vickers hardness instrument at the load of 5N and the dwell time of 15s.

Wear tests were conducted on a multi-functional tribometer (UMT-2) at room temperature. The sintered specimens was used as the disc and the size is 20 mm and 5 mm in diameter and thickness, respectively. The counterpart was the stainless ball produced from GCr15steel and the friction diameter was 4mm, and its' hardness was HRC63. Prior to each test experiment, the surface of the stainless ball and specimens were processed and cleaned with acetone. The wear tests were set at the sliding speed of 200 rpm (0.0612 m/s), at the test time of 30 min and an appiled load of 5 N. The wear rate was expressed as the wear volume divided by the applied load and sliding distance.Further, all tests were repeated under the same condition at least four times.

3. Results and discussion

3.1. Characterization

The microstructure of $NbSe_2$ and GO are shown in Fig.2. It could be seen that $NbSe_2$ product consisted of a large number of microplates exhibiting a hexagonal structure, which exhibited the average diameter about 3μm and 400 nm in thickness(Fig.2a). The TEM image of $NbSe_2$ taken from microplates is given in Fig.2b, the results corresponded to the result of $NbSe_2$ possessing a hexagonal structure. In order to study the structure in details, the [0001] zone-axis HRTEM as well as the SAED pattern of $NbSe_2$ is indicated in Fig.2c-d. The lattice fringe of $NbSe_2$ with a typical hexagonal structure had a spacing of 0.62nm consistent with the theoretical d–spacing for (002) planes. Besides, the SAED pattern further showed the single crystalline nature of the hexagonal flake and $NbSe_2$ grew normal to [0001] direction[19]. Fig.3 shows the SEM and TEM images of GO. It clearly demonstrated that synthesized GO nanosheets, curled and winkled, were flake structures with some foldings.

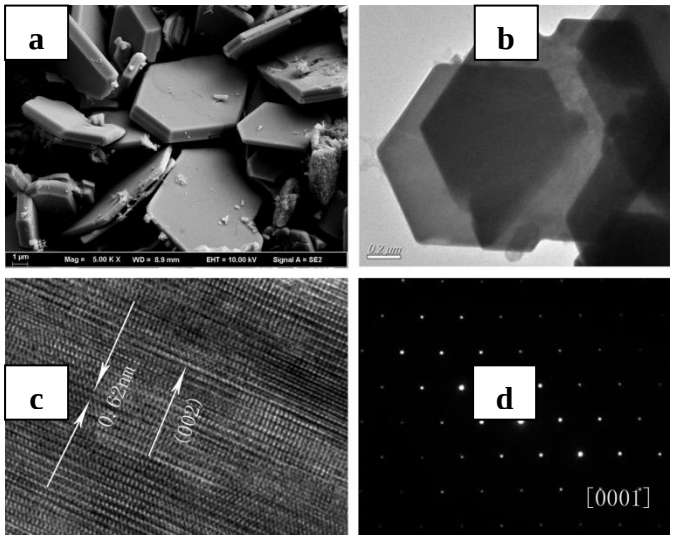

Fig.2. SEM image of $NbSe_2$ microplates (a), TEM pattern of $NbSe_2$ microplates (b), HRTEM pattern of $NbSe_2$(c) and SAED pattern of $NbSe_2$ microplates(d)

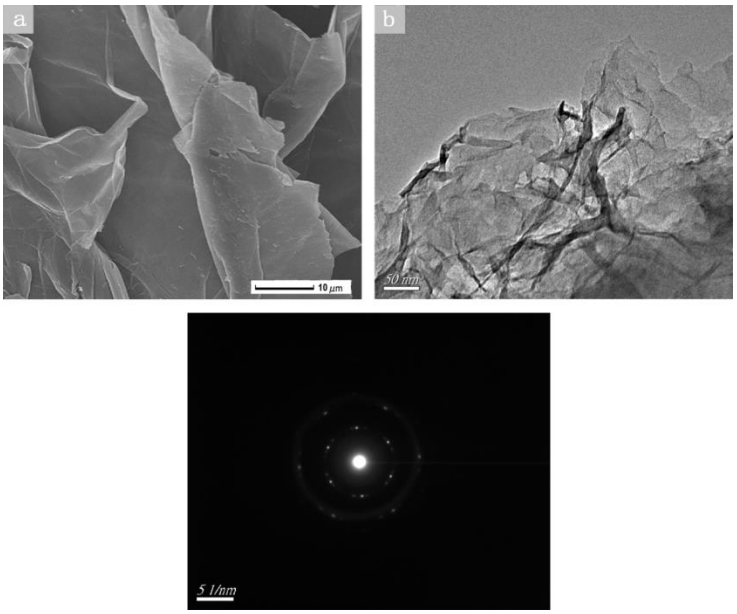

Fig. 3. SEM image of GO (a) ,TEM pattern of GO (b) and SAED pattern of GO nanosheet(c)

The phase constituents of $NbSe_2$ and GO were identified by XRD, and results are illustrated in Fig.4. All observed diffraction peaks of $NbSe_2$ could be indexed to hexagonal $NbSe_2$ phase (JCPDS No.65-7464)with calculated lattice constants of a=3.445Å and c=12.55Å. Other peaks from impurities were not detected, indicating that the $NbSe_2$ was of high purity. GO had two strong diffraction peaks: one was at about 2θ = 9.8°, relating to (001) reflection peak, which was due to the formation of intercalated water moieties and oxygen functionalities groups between the layers of GO [20]. And another mild peak at around 20° could be the characteristic peak (002) plane reflections of graphite from the graphene (JCPDS no.01-0646) [21]. The (002) crystal plane was very broad, suggesting that the sample was very disorderedly along the stacking direction.

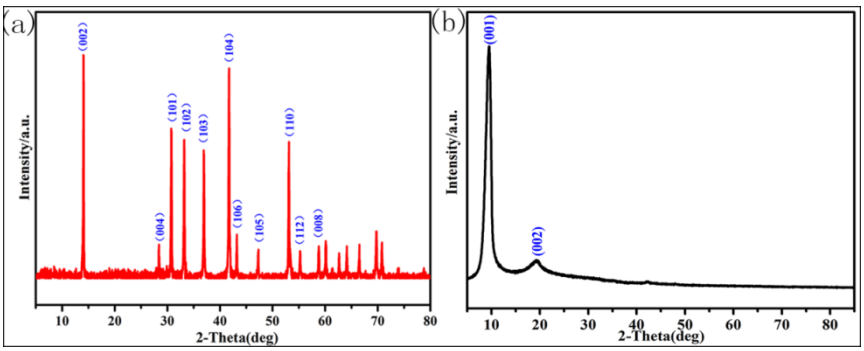

Fig.4. XRD patterns of $NbSe_2$(a) and GO(b)

3.2. Phase composition, microstructure, hardness and density

Fig.5 shows the XRD patterns of Cu-based composites. Results that copper were the main phases in all sintered composites and the $NbSe_2$ phase disappeared. Cu_xNbSe_2 as well as a small amount of Cu_2Se phases were observed, which suggested that most $NbSe_2$ reacted with copper and transformed into Cu_xNbSe_2 and Cu_2Se during the sintering process[19]. However, the diffraction peaks of RGO could not be detected, which might be the strong peaks of copper covered up the diffraction peaks of RGO [13].

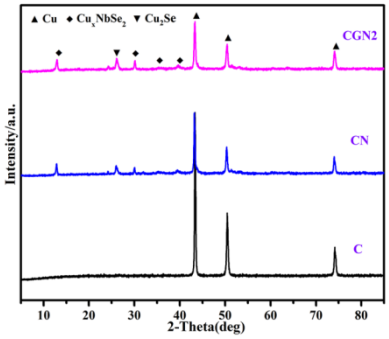

Fig.5. XRD patterns of as-prepared C, CN and CGN2

In addition, Fig. 6 further exhibits the microstructure and elemental distribution of specimen CGN2 composite. It could be seen that the dense microstructure was evenly composed of three obvious phases: the gray, deep gray as well as dark regions, respectively. According to the elemental distribution, the deep gray region was rich in Cu,Nb,Se and gray region was rich in Cu while the dark region was rich in C. Combining the results of XRD and Raman spectra technique, the deep gray, gray and dark region were Cu, Cu_xNbSe_2/$NbSe_2$ and RGO, respectively. It could also be noted that the RGO exhibited both agglomerated and dispersed states.

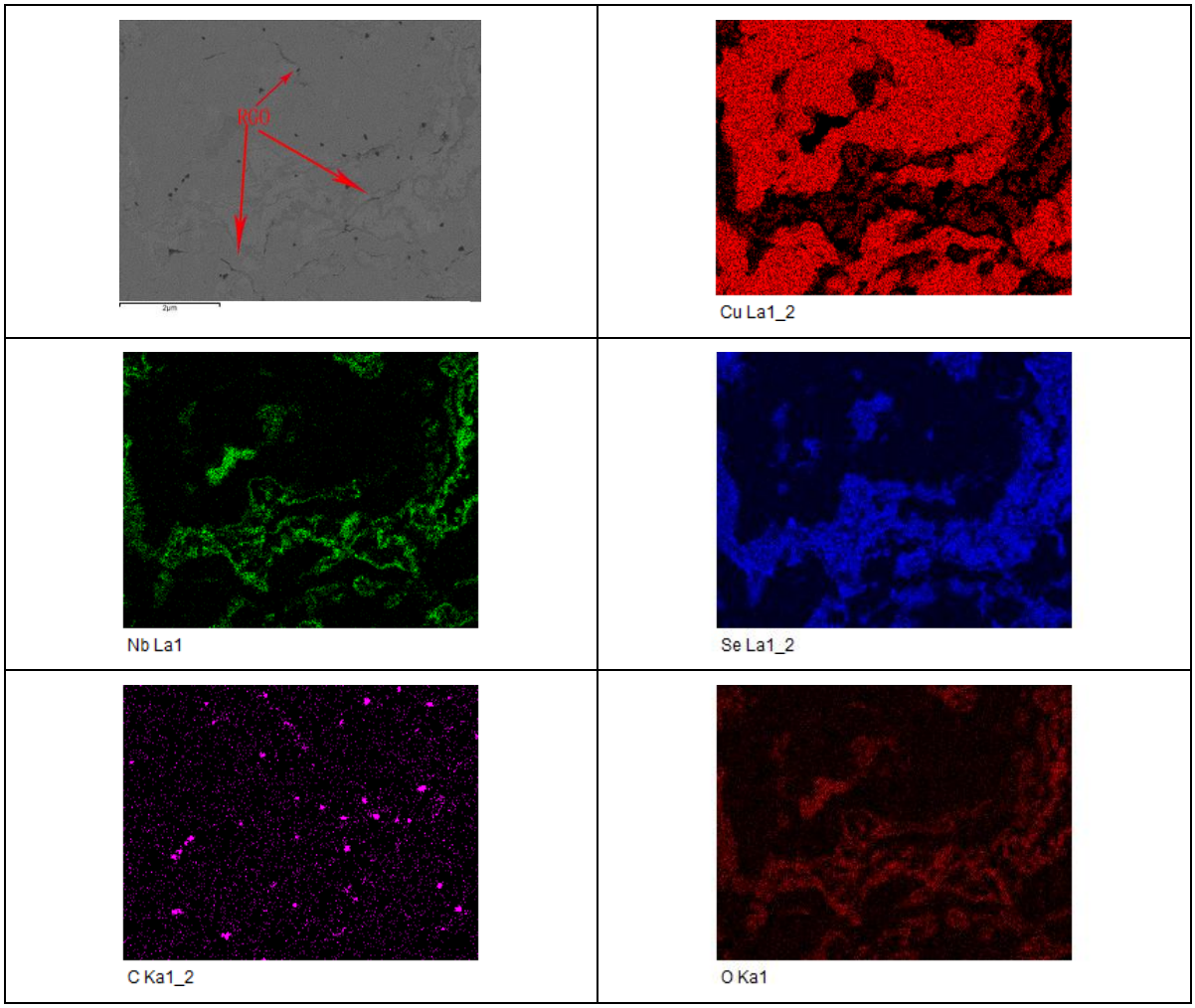

Fig. 6. Microstructure and elemental distribution of specimen CGN2

Table 1. The chemical compositions, density and micro-hardness of Cu-based composites in mass

Specimen	Cu	RGO	$NbSe_2$	Sintered density (g/cm^3)	hardness (HV)
C	100	0	0	7.31	75
CN	80	0	20	7.27	103
CGN1	80	1	19	7.18	107
CGN2	80	2	18	7.11	112
CGN3	80	3	17	7.04	104

Table 1 lists the compositions, hardness and sintered density of Cu-based composites. Specimen C had a density of $7.3g/cm^{-1}$ and an average hardness of 75HV. Specimen CN showed a higher hardness of 103HV than specimen C, suggesting that the hardness of composites was greatly enhanced by the addition of $NbSe_2$ [10]. The hardness of specimen CGN1, CGN2 and CGN3 increased compared with specimen CN due to the addition of RGO with the excellent mechanical properties[13,22]. However, the hardness of specimen CGN3 was lower than that of specimen CGN2, which might be mainly because excess of RGO led to much agglomeration. The agglomeration of RGO deteriorated the mechanical properties of composites[23]. The introduction of low density of RGO or $NbSe_2$ led to the sintered density of composites decreased.

3.3. Tribological properties

Fig.7 presents the variation of friction coefficients and wear rates of Cu-based composites under dry friction. For Fig.7a, It was clear that the specimen C had the highest friction coefficient about 0.55 at a unsteady state among all samples. As expected, the friction coefficient of Cu-based composites sharply decreased from 0.55 to 0.23 with the addition of $NbSe_2$, which were more stable than that of specimen C, but had a upward trend. This was mainly because of the excellent lubricity of $NbSe_2$ determined by its laminated structure[10]. In addition, the friction coefficient of composites were lower and fluctuated more slightly than those of specimen C and CN with the introduction of RGO. Especially, the friction coefficient of specimen CGN2 showed the lowest and most stable friction coefficient. The results found that the anti-friction properties of Cu-based composites were remarkably enhanced by the addition of RGO. However, with the content of RGO further increasing to 3wt.%, the friction coefficient of speciemn CGN3 tended higher value, which might be related to the agglomeration of RGO. Furthermore, the changing trend of friction coefficients were almost the same as wear rates. For Fig.7b, the wear rate of specimen C was about $6.5\times10^{-3}mm^3.N^{-1}m^{-1}$. However, the wear rate of composites (specimen CN) was as low as about $3.5\times10^{-3}mm^3.N^{-1}m^{-1}$ with the introduction of $NbSe_2$, which sharply decreased by 46% compared with specimen C. The addition of $NbSe_2$ could effectively enhance the wear resistance of copper-based composites[8]. As a result of the reinforcement effect of RGO, the antiwear properties of copper-based composite with $NbSe_2$ (specimen CGN1) was further enhanced by RGO[13]. Besides, specimen CGN2 possessed the lowest wear rate about $0.07\times10^{-3}mm^3.N^{-1}m^{-1}$, which was almost decreased by more than 98% in comparsion with specimen C. Similarly, as the RGO increased to 3 wt.%, the wear rate of Cu-based composite sightly increased, which might be because the excess of RGO ocurred some agglomeration so that deteriorated the hardness of Cu-based composite, and the reduction of hardness was a key factor in decreasing the wear resistance[19,24]. That is, filling 2 wt.% RGO led to composites possess the lowest friction coefficient and wear rate. For the reason why the tribological properties of composites greatly improved by means of filling $NbSe_2$ and RGO, it could be ascribed to two points. One was $NbSe_2$ and RGO provided good lubricity like MoS_2 and graphite. Another was the increase of hardness decreased the friction coefficient and wear rate[25].

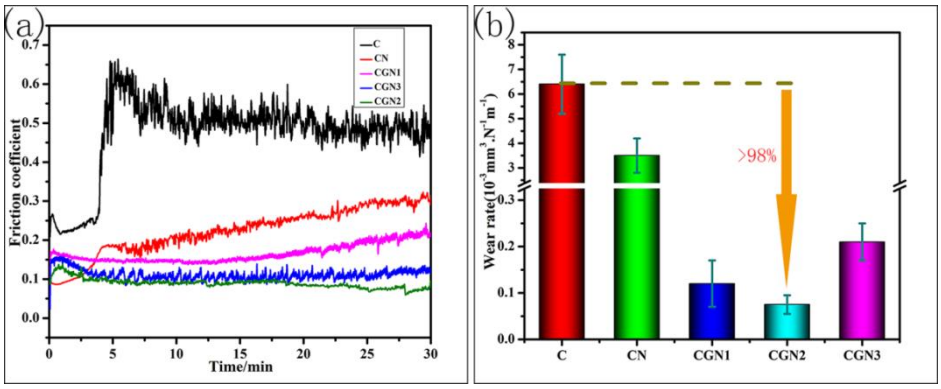

Fig. 7. Friction coefficients and wear rates of Cu-based composites sliding against stainless steel ball under dry friction

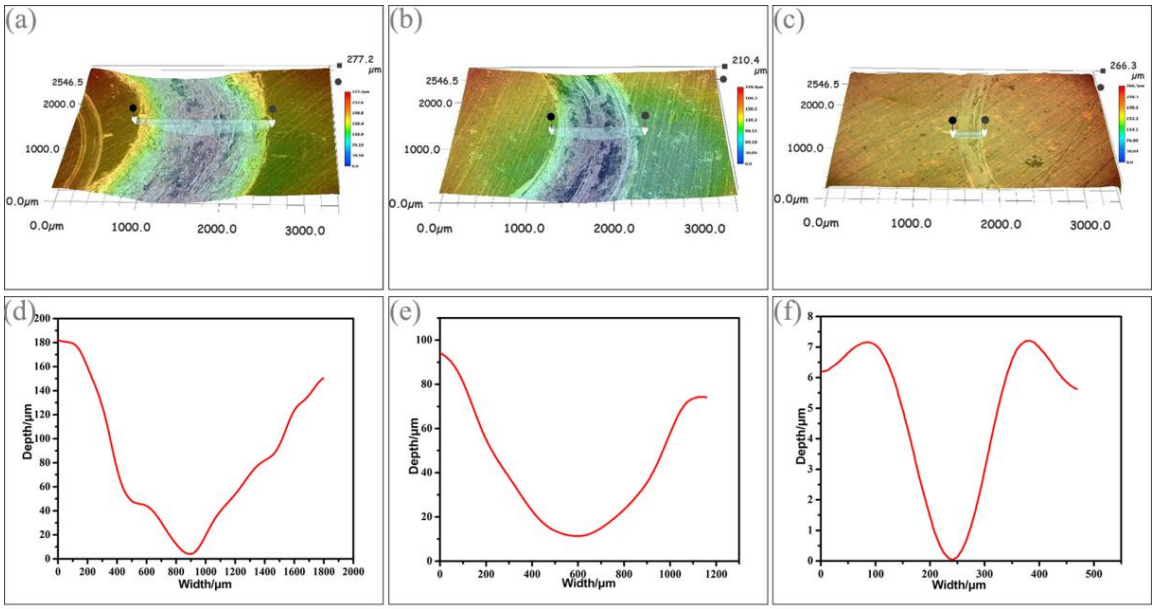

Fig. 8. Noncontact three-dimensional cross-section images of wear tracks obtained on surface of specimen C (a), specimen CN (b) and specimen CGN2 (c) under the applied load of 5 N; (d, e, f) Corresponding cross-section profiles of the wear tracks

To further verity specimen CGN2 possessing excellent tribological properties among all speciemns. Fig.8 illustrates noncontact three-dimensional cross-section images of wear tracks. It could be clearly seen that the depth and width of the wear scar for specimen C were about 170 μm and1.8 mm respectively, while specimen CN were about 82 μm and 1.2 mm. Particularly, the depth and width of the wear scar for specimen CGN2 were about 7.5 μm and 0.45 mm respectively and the wear scar in Fig.8c was obviously light and smooth compared with that in Fig.8a and Fig.8b. Above all, Specimen CGN2 showed the excellent tribological properties due to the combined effect between $NbSe_2$ and RGO, which was consistent with in Fig.7b.

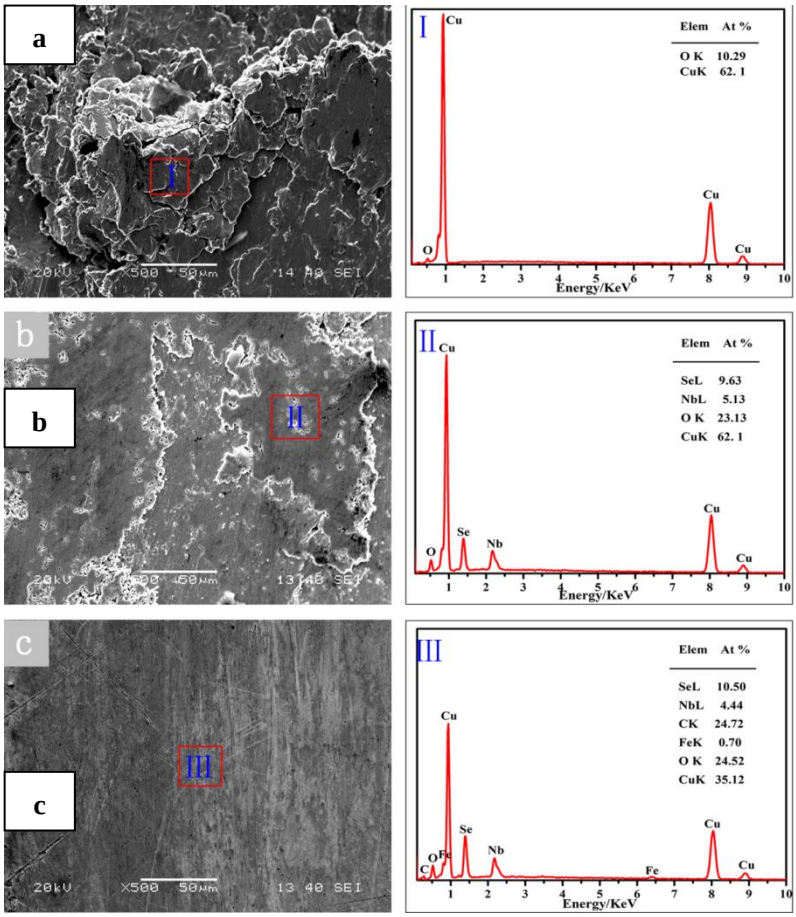

Fig.9. SEM micrographs of specimen C, CN and CGN2 (5N load, 6.12cm/s). (a)-(c) represented the worn surface of C, CN and CGN2, respectively. (I)-(III) represented EDS result of the worn surface of C,CN and CGN2

3.4 Evaluation of worn surfaces

Fig. 9 shows the worn surfaces of composites after wear test. As can be seen in Fig.9a. pure copper suffered serious wear evidenced by clear adhesive and serious plastic deformation on the worn surface, indicating that adhesive wear and serious plastic delamination was the main wear mechanism, which was consistent with the result of pure copper possessing the highest wear rate. The worn surface of specimen CN seemed to be milder than that of specimen C. Plastic deformation and adhesion phenomenon on the worn surfaces of specimen CN were restricted due to the addition of $NbSe_2$[8,10]. Furthermore, apart with small amount of plastic deformation, slight delamination was formed on the worn surface of specimen CN, which matched well with lower friction coeffient and wear rate. For specimen CGN2 (Fig.9c), The adhesion and phastic deformation were not found on the worn surface, which, exhibiting the most smooth area with the very shallow grooves, formed the continuous and homogenous tribo-film, which accounted for the lowest friction coefficient and wear rate. This might be because $Cu_xNbSe_2/NbSe_2$ with low shearing stress were squeezed out from Cu matrix to form the tribo-film during the sliding process, which led to a low friction coefficient[26]. And RGO penetrated into the very narrow grooves and gaps on the tribo-film between the asperities of sliding contact, which could change the direct contact area of the tribo-film-the asperities of counterpart to the tribo-film-RGO-the asperities of counterpart. The plowing effect of the asperities of counterpart could be greatly resisted to protect the tribo-film from further damage due to the presence of RGO nanosheets with high hardness, which was consistent with some reports[26-28].

The EDS analysis of the area marked by a rectangle on the worn surface of specimens C, CN and CGN2 are shown in Fig.9 (I-III). For specimen CGN2, the peaks of C, Nb, Se were detected apart with Cu peak and the atom ratio of Nb and Se elements was close to 1:2, which indicated the formation of the tribo-film[26]. However, the low Intensity oxygen and Fe peaks also were found due to some oxides formation occured on the worn surface. It was believed that the oxides, RGO and Cu_xNbSe_2/$NbSe_2$ coexisted in the tribo-film, which were responsible for friction reduction.
Specimen CGN2 with excellent tribological properties was chosen for further analysis for determining the anti-wear mechanism of Cu-based composites. Fig.10 displays Raman spectrum of the unworn surface and worn surface of specimen CGN2. Few peak of $NbSe_2$ was detected on the surface of specimen CGN2 before wear test. However, $NbSe_2$, Fe_2O_3, CuO and RGO were observed on the tribo-film of specimen CGN2 and the peak of $NbSe_2$ became more and more obvious after wear test, which demonstrated more $NbSe_2$ was reformed on the worn surface. CuO and Fe_2O_3 was formed by oxidation of Cu, and Fe transferred from the counterpart[24,29] due to the effect of friction heat. $NbSe_2$ was reproduced by the decomposition of Cu_xNbSe_2. The formation of oxides and reformation of $NbSe_2$ accounted for the reduction of friction coefficient and wear rate during the rubbing process[26]. Besides, the position of the A_{1g} peak of $NbSe_2$ with noticeable angular widening of the relative profiles shifted negatively from about 230cm^{-1} to 215cm^{-1} after wear test compared with the position of A_{1g} peak of as-prepared $NbSe_2$, which meant the inplane structure of $NbSe_2$ was greatly broken. Above all, $NbSe_2$ were sheared into thiner sheets in the process of friction and wear, which was mainly ascribed to $NbSe_2$ with a typical lamellar structure was easily sheared due to van der Waals force between the layers [9,28].

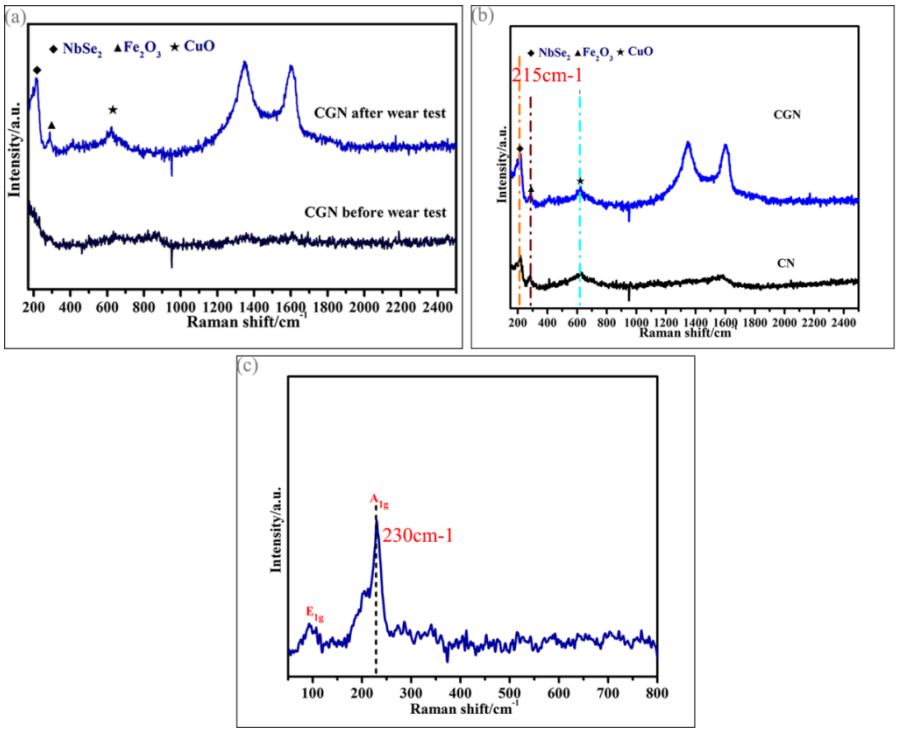

Fig.10. Raman spectrum of the worn surface of specimen CGN2 before and after wear test(a) and the worn surface of specimen CN and CGN2(b), $NbSe_2$ (c)

Fig. 11 provides the chemical states of Cu,Nb,Se,C and Fe elements on the worn surface of specimen CGN2. Fig.11a shows that XPS results of the worn surface of specimen CGN2, the observed areas found six relatively strong peaks. In Fig.11b, XPS spectra peaks of Cu 2p were loacated at 953.7eV and 932.9eV, which were associated with CuO and Cu_2Se, respectively[19,30]. Similarly, the Nb 3d spectrum could be resolved into three binding energy peaks of 202.3 eV,

207.4 eV and 210.2eV, which were corresponded to the Nb 3d $_{5/2}$, Nb 3d $_{3/2}$ and Nb 3d $_{5/2}$ chemical states in $NbSe_2$ and Nb_2O_5, respectively (Fig.11c). The Se 3d spectrum also could be resolved into two binding energy peaks of 54.2 eV and 55.2eV, which could be corresponded to Cu_2Se and $NbSe_2$ respectively (Fig.11d). The C 1s spectrum showed four peaks at 284.5 eV, 285.1 eV, 285.9 eV and 287.5 eV, which could be attributed to the carbon atoms in different functional groups: C=C, C-C, C-O and C=O, respectively (Fig.11e). This could be associated with RGO[31]. Besides, the peak of Fe 2p around 710 eV and 720 eV, which were assigned to the Fe 2p $_{3/2}$ and Fe 2p $_{1/2}$ chemical states in Fe_2O_3 and Fe, respectively (Fig.11f)[30]. The tribo-film mianly consisted of $NbSe_2$, RGO, Cu-Fe-Nb-oxides and Cu_2Se, which was consistant with micro-Raman and EDS results. It could be concluded that wear process promoted the formation of oxides, and formation of tribo-film was remarkable improved the friction-reducing and anti-wear properties of Cu-based composites[24].

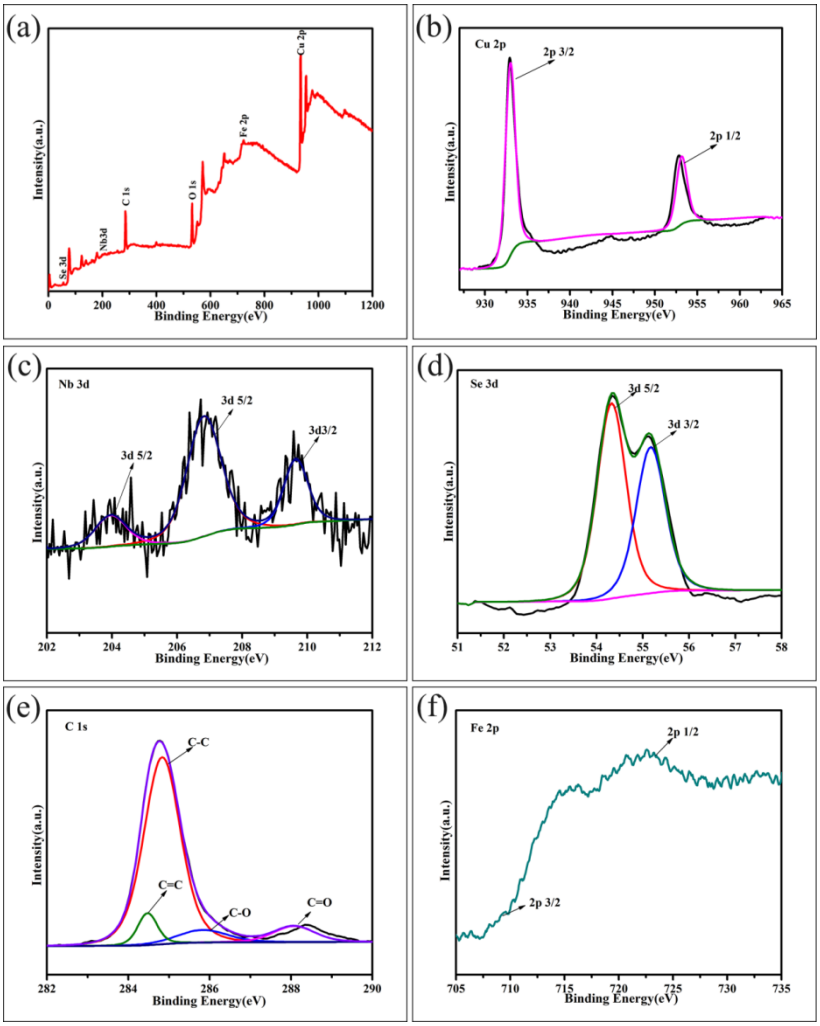

Fig.11. XPS spectra on the worn surface of specimen CGN2 after wear test

4. Conclusions

The addition of $NbSe_2$ and RGO decreased the density, but increased hardness of copper. The strengthing effect of RGO was better than that of $NbSe_2$. Cu-based composites with $NbSe_2$

and RGO exhibited the excellent tribological properties, especially, Cu-based composites containing 18wt.%$NbSe_2$ and 2wt.%RGO possessed the best tribological properties among all other samples. EDS, Raman and XPS analysis suggested that the dense and complete tribo-film, consisting of Fe_2O_3, CuO, Nb_2O_5, RGO and $NbSe_2$ significantly improved the tribological properties.

Acknowledgements

This work was financially supported by National Natural Science Foundation of China (51275213, 51302112), the Jiangsu National Nature Science Foundation (BK2011534, BK2011480), the Scientific and Technological Innovation Plan of Jiangsu Province in China (Grant Nos. CXLX13_645).

References

[1] X. Li, G.P. Song, F.Y. Bu, B. Xu, B.Y. Lou, Z. Lin, Rare Mel. **33**, 568 (2014).
[2] K. Rajkumar, S Aravindan, Tribol Int . **44**, 347 (2011).
[3] H.M. Zhang, X.B. He, X.H. Qu, Q. Liu, X.Y. Shen, Rare Met. **32**, 75 (2013).
[4] X.H. Zhang, C.G. Lin, S. Cui, Z.D. Li, Rare Met. **33**, 191(2014).
[5] R. Manory, Wear. **249**, 626 (2001).
[6] G. Cui, Q. Bi, M. Niu, J. Yang, W. Liu, Tribol. Int. **60**, 25 (2013).
[7] J. Zeng, J. Xu, W. Hua, L. Xia, X. Deng, S. Wang, P. Tao, X. Ma, J. Yao, C. Jiang, L. Lin, Appl. Surf. Sci. **255**, 6647(2009).
[8] G. Cui, Q. Bi, J. Yang, W. Liu, Mater. Des. **46**, 473 (2013).
[9] S. Chen, H. Li, H. Tang, Y. Zhang, J. Yang, X.R. Ji , Cryst. Res. Technol. **49**,152 (2014).
[10] H. Tang, K. Cao, Q. Wu, C. Li, X. Yang, X. Yan, Cryst. Res. Technol. **46**,195 (2011).
[11] BeiBei Chen, Jin Yang, Qing Zhang, Hong Huang, Hua Tang, ChangSheng Li, Material and Desgin. **75**, 24(2015).
[12] R.G. Zheng, X.M.Liu, Materials Research Innovations.**18**,31(2014).
[13] Lee C, Wei XD, Kysar JK, Hone J, Science.**321**,385(2008)
[14] Xinjiang Zhang, Pengyu Dong, Yong Chen, Wenchao Yang, Yongzhong Zhan, Kaifeng Wu, Yueyu Chao, Tribology International. **103**,406 (2016)
[15] Mingsuo Zhang, Beibei Chen, Jin Yang, Hongmei Zhang, Qing Zhang, Changsheng Li, RSC Ad. **5**, 89682 (2015)
[16] W. Li, L. Hu, M. Wang, H. Tang, C. Li, J. Liang. Li, Cryst. Res. Technol. **47**,876 (2012)
[17] X. Zhang, D. Zhang, H. Tang, X. Ji, Y. Zhang, G. Tang , Mater. Res. Bull. **53**,96 (2014)
[18] W.S. Hummers, R. E. Offeman, J. Am Chem Soc. **80**, 1339 (1958)
[19] Q. Shi, J. Yang, W. X. Peng, Rsc Advances. **5**, 100472 (2015).
[20] S. F Pei, Cheng HM, Carbon. **50**, 3210 (2012).
[21] K. Gotoh, T. Kinumoto, E. Fujii, A. Yamamoto, Carbon.**49**,1118 (2011).
[22] Dandan Zhang, Zaiji Zhan, Journal of Alloys and Compounds. **654**, 226(2016).
[23] Jing-fu Li, Lei Zhang, Jin-kun Xiao, Ke-chao Zhou,Trans.Nonferrous Met.Soc China.

25, 3354(2015)
[24] Eryong Liu, Yaping Bai, Yimin Gao, Gewen Yi, Junhong Jia, Tribology International. **80**, 25 (2014).
[25] Xinghua Zhang, Jun Cheng, Muye Niu, Hui Tan, Weimin Liu, Jun Yang, Tribology International. **101**, 81(2016).
[26] Hongping Li, Lin Chen, Yi Zhang, Xiaorui Ji, Shuai Chen, Changsheng Li , Cryst. Res. Technol. **49**, 204 (2014)
[27] H. Huang, J. Tu, L. Gan, C. Li, Wear. **261**, 140 (2006).
[28] A. D. Moghadam, E. Omrani, P. L. Menezes, P. K. Rohatgi, Compos Part B.**77**, 402 (2015).
[29] Gongjun Cui, Lei Lu, Juan Wu,Yanping Liu, Guijun Gao, Joural of Alloys and Compounds. **611**,235(2014)
[30] Kongjie Jin, Zhuhui Qiao, Shengyu Zhu, Jun Cheng, Bing Yin, Jun Yang, Tribology International. **98**, 1 (2016)
[31] Zhengyan Chen, Hongxia Yan, Tianye Liu, Song Niu, Composites Science and Technology. **125**, 47 (2016).